JACS
JOURNAL OF THE AMERICAN CHEMICAL SOCIETY
Communication
pubs.acs.org/JACS

Rolling Up Gold Nanoparticle-Dressed DNA Origami into Three-Dimensional Plasmonic Chiral Nanostructures

Xibo Shen,[†] Chen Song,[†] Jinye Wang,[†] Dangwei Shi,[†] Zhengang Wang,[†] Na Liu,*[,‡] and Baoquan Ding*[,†]

[†]National Center for Nanoscience and Technology, Beijing 100190, China

[‡]Department of Electrical and Computer Engineering, Rice University, 6100 Main Street, Houston, Texas 77005, United States

Supporting Information

ABSTRACT: Construction of three-dimensional (3D) plasmonic architectures using structural DNA nanotechnology is an emerging multidisciplinary area of research. This technology excels in controlling spatial addressability at sub-10 nm resolution, which has thus far been beyond the reach of traditional top-down techniques. In this paper, we demonstrate the realization of 3D plasmonic chiral nanostructures through programmable transformation of gold nanoparticle (AuNP)-dressed DNA origami. AuNPs were assembled along two linear chains on a two-dimensional rectangular DNA origami sheet with well-controlled positions and particle spacing. By rational rolling of the 2D origami template, the AuNPs can be automatically arranged in a helical geometry, suggesting the possibility of achieving engineerable chiral nanomaterials in the visible range.

Advanced designs of nanomaterials require a large amount of control over the assembly of nanoscale components. Structural DNA nanotechnology, which utilizes the programmability of DNA, offers a compelling approach leading toward fully addressable nanopatterning.[1,2] In particular, the DNA origami technique can create arbitrary 2D or 3D DNA nanoarchitectures with well-defined sizes, shapes, and spatial addressability.[3−12] The process involves programmable folding of a viral single-stranded DNA (ssDNA) by numerous helper strands.[5] Because each individual helper strand can be modified and extended to produce a sequence-dependent surface tag, DNA origami has been utilized as a template to assemble functionalized metallic and semiconducting nanocrystals, carbon nanotubes, and biological materials into sophisticated geometries.[13−21] In addition, DNA origami can carry addressable binding sites at a resolution of ∼6 nm, which is far smaller than the features obtained using traditional electron-beam lithography. Most remarkably, DNA origami allows for rational 3D organization of nanocrystals, which remains a significant challenge for top-down techniques.[22,23]

Among a variety of nanocrystals, metallic nanoparticles (NPs) have been of great interest because of their unique optical properties. A metallic NP supports localized surface plasmons, which are associated with the collective oscillation of the conductive electrons in the NP. The strong interactions of plasmons in NP assemblies render possible many useful applications, including surface-enhanced spectroscopies, sub-wavelength optical devices, and medical diagnostics and therapeutics. Considerable effort has been devoted to organizing metallic NPs into sophisticated plasmonic architectures using DNA origami. Yan and co-workers were the first to use DNA origami to assemble multiple AuNPs.[24] These researchers also demonstrated encapsulation of AuNPs in a DNA origami cage.[25] Pilo-Pais et al.[26] used DNA origami to create predesigned AuNP assemblies, including rings, parallel bars, and H shapes. In our previous work, we constructed linear AuNP chains that could work as a nanolens on triangular DNA origami templates.[15]

Recently, plasmonic chiral materials have attracted a lot of attention.[27] Natural chiral molecules such as proteins and DNA exhibit strong optical chirality only in the UV range. Theoretical calculations have shown that plasmonic assemblies consisting of metallic NPs that are arranged in chiral geometries such as pyramids, tetrahedrons, helices, etc.,[28] provide a unique way to achieve strong optical chirality in the visible range. At resonance, the dipolar plasmons of individual metallic NPs can be strongly coupled. The collective plasmons that oscillate along a plasmonic chiral structure of certain handedness can lead to different absorptions in response to right- and left-circularly polarized light [i.e., circular dichroism (CD)]. Over the past several years, different approaches have been directed toward organizing AuNPs into chiral 3D geometries. Natural chiral materials such as peptide−amphiphile supramolecules were utilized as scaffolds to grow AuNPs directly through gold nucleation from precursor salt solutions.[29] The geometries of the resulting gold helices, however, were not easily engineerable in that they followed the same morphology of the natural peptide-based materials. Another strategy is associated with self-assembly of DNA tubules through integration of AuNPs.[30] Stacked rings, spirals, and nested spiral tubes were obtained by utilizing size-dependent steric repulsion effects among AuNPs. Nevertheless, chiral gold structures of a certain conformation could not readily be separated from the product mixture. In 2009, Mastroianni et al.[31] demonstrated a chiral grouping of four different-sized AuNPs that were monofunctionalized with distinct strands of DNA. Because of the substantial size difference, however, the four AuNPs could not be efficiently coupled. In this case, optical chirality was thus not expected according to theoretical calculations.[28]

In this communication, we demonstrate the construction of 3D plasmonic chiral nanostructures through programmable transformations of AuNP-dressed DNA origami. A 2D

Received: October 20, 2011
Published: December 12, 2011

   dx.doi.org/10.1021/ja209861x | J. Am. Chem.Soc. 2012, 134, 146−149

rectangular DNA origami template is functionalized with two linear AuNP chains at specific positions. The process is then followed by rationally rolling and stapling the 2D DNA rectangular origami into tubular DNA origami. After rolling, the AuNPs are automatically organized into a 3D helix on the tubular DNA origami. The 3D plasmonic helix composed of nominally identical AuNPs resembles natural chiral biomolecules such as proteins and DNA. Our strategy holds great promise for the creation of chiral plasmonic nanomaterials with engineerable optical chirality.

Figure 1 illustrates the experimental scheme. A rectangular DNA origami template composed of 24 DNA helices was first

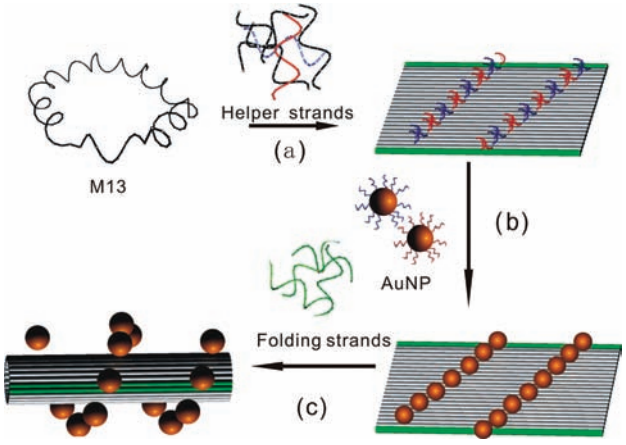

Figure 1. Illustration of the experimental scheme. (a) A long ssDNA scaffold (M13, in black) hybridizes with helper strands to form a 2D rectangular DNA origami template that has binding sites on only one surface. These binding sites are well-positioned along two linear chains. To avoid nonspecific binding, different-sequence capture strands (in red and blue) are placed alternatively at the binding sites. (b) AuNPs (10 nm) covered with corresponding DNA strands are assembled at the predesigned locations on the origami sheet through complementary strand hybridization. The sequence of the two long sides of the rectangular DNA origami (in green) is modified to be complementary to that of the folding DNA strands. (c) Addition of the folding strands leads to rolling and subsequent stapling of the 2D rectangular origami sheet into a hollow DNA origami tube. As a result, the AuNPs are automatically arranged into a 3D helix.

prepared following the scaffolded DNA origami method developed by Rothemund.[5] The dimensions of the 2D origami were 90 nm × 60 nm × 2 nm. DNA capture strands with carefully designed sequences were extended from the rectangular DNA template at specific positions. After hybridization of the rectangular DNA origami template, all of these capture strands were displayed on one side of the template. We had altogether 15 binding sites that were arranged along two parallel lines, as shown in Figure 1. At each binding site, three identical-sequence capture strands were used to localize one single AuNP (10 nm) precisely. To avoid nonspecific binding, different-sequence capture strands (in red and blue) were placed alternatively at the binding sites. The AuNPs were functionalized with corresponding complementary DNA strands. The spacing between the individual AuNPs along each chain (16 nm) was controlled by the positions of the capture DNA strand groups. The sequence of the two long sides of the rectangular DNA origami (in green) was modified to be complementary to that of the folding DNA strands. Upon the addition of the DNA folding strands, the rectangular origami sheet started to roll up. Eventually, the two long sides of the 2D DNA origami sheet were stapled together, giving rise to a hollow DNA origami tube. As a result, the AuNPs were arranged in a helical geometry on the hollow origami tube, as illustrated in Figure 1.

The 2D rectangular DNA origami was obtained by annealing the M13 strand, capture strands, and helper strands in a ratio of 1:2:10 from 90 °C to room temperature. The product was then purified using a filter device [100 kDa molecular weight cutoff (MWCO), Amicon, Millipore] to eliminate the extra DNA strands. To demonstrate the effectiveness of the rolling process, the folding DNA strands were added to the DNA origami structures in a 50:1 ratio to transform the 2D origami sheets to hollow DNA tubes. The samples were analyzed by agarose gel electrophoresis. The gel image is presented in Figure 2a. Lanes

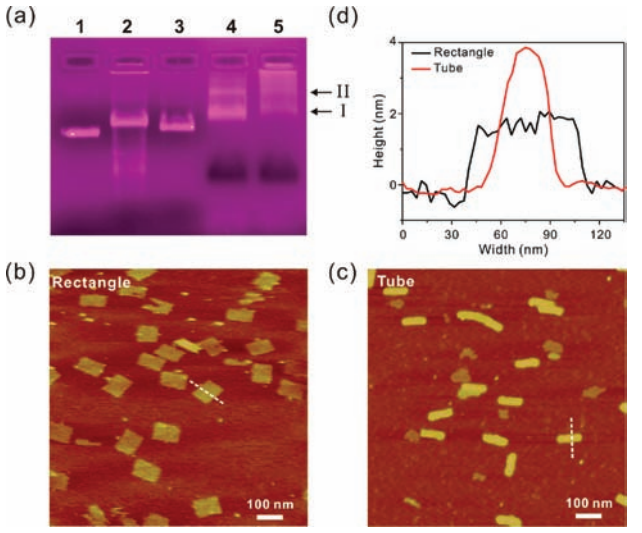

Figure 2. (a) Ethidium bromide-stained agarose gel of the products at different experimental stages. Lane 1: M13. Lane 2: rectangular DNA origami. Lane 3: tubular DNA origami. Lane 4: rectangular DNA origami dressed with AuNPs. Lane 5: DNA origami tube dressed with AuNPs. Bands 4I and 5I are the target products, and bands 4II and 5II are aggregates of multiple DNA origami. (b, c) AFM images of the (b) rectangular and (c) tubular DNA origami. (d) AFM measurements of the heights and widths of the DNA origami rectangle and tube.

1 and 2 correspond to the M13 strand and the 2D rectangular DNA origami, respectively. The 2D rectangular DNA origami has a lower mobility than the M13 strand because of hybridization of the M13 strand with the helper and capture strands. Lane 3 contains the tubular DNA origami. After rolling, the tubular DNA origami became more tightly packed, elevating its running speed in the gel. Lane 3 is hence located at a lower position with respect to lane 2, as shown in Figure 2a. Atomic force microscopy (AFM) was used to visualize the rectangular and tubular DNA origami structures. Figure 2b shows the rectangular DNA origami; the sheet-like structures are clearly visible. Figure 2c shows the tubular DNA origami. To characterize these DNA structures further, the widths and heights of the products were measured by AFM. The widths of the rectangular and tubular origami were ~60 and ~30 nm, respectively (Figure 2d), consistent with our design. The tube height was ~3.8 nm, which is about twice the height of the 2D rectangular origami (1.8 nm). The measured height was much smaller than the tube diameter (23 nm) because the hollow

dx.doi.org/10.1021/ja209861x | J. Am. Chem.Soc. 2012, 134, 146–149

DNA origami tubes collapsed during the drying process on the substrate for AFM imaging.

AuNPs (10 nm) were fully modified with 15 nucleotide (nt) thiolated ssDNA (5′-TTTTTTTTTTTTTTT-S-3′ and 5′-ATTATTATTATTATT-S-3′). The functionalized AuNPs were then purified using the same method as applied to the rectangular DNA origami for removing the unbound oligonucleotides. Subsequently, the rectangular DNA origami was mixed with the modified AuNPs in a ratio of 1:30. The mixture was slowly annealed from 40 °C to room temperature in order to assemble AuNPs at the predesigned positions on the origami surface. Next, the folding DNA strands were added to the rectangular DNA origami in a 50:1 ratio for stapling. The assembled AuNP/DNA origami products before and after transformation were also analyzed by agarose gel electrophoresis. After conjugation with AuNPs, both the rectangular and tubular origami showed less mobility than the bare rectangular origami (Figure 2a, lanes 4 and 5).

The two target gel bands 4I and 5I (see Figure 2a) were then sliced and extracted by electroelution with dialysis tubing membranes (50 kDa MWCO) and imaged by transmission electron microscopy (TEM). Figure 3a shows TEM images of

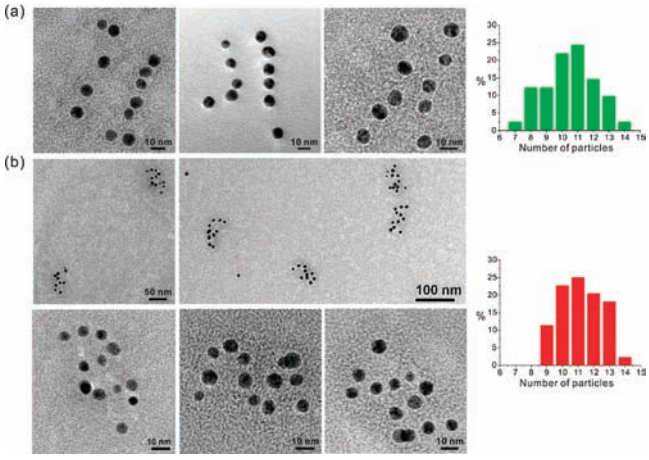

Figure 3. (a) TEM images of the rectangular DNA origami dressed with two chains of AuNPs. (b) TEM images of the tubular DNA origami dressed with AuNPs, which form 3D AuNP helices. Histograms of the numbers of AuNPs assembled on the rectangular and tubular DNA origami are shown on the right in (a) and (b), respectively.

the rectangular DNA origami dressed with two AuNP chains. Some missing binding sites along the chains are observable. This is likely due to the steric and electrostatic repulsion among the AuNPs, which were all functionalized with negatively charged DNA (15 nt, ~5 nm long). The two chains on the DNA origami are not completely straight in that the assembled AuNPs deformed the flatness of the 2D rectangular DNA origami during the drying process on the TEM grid. The TEM images of the tubular DNA origami/AuNP complexes (Figure 3b) demonstrate the formation of 3D AuNP helices. In these TEM images, the average length, pitch, and diameter of the AuNP helices are approximately 71, 37, and 33 nm, which are consistent with our design. Histograms of the numbers of AuNPs assembled on the rectangular and tubular origami structures (Figures 3a and 3b, respectively) show that there is a higher probability of having larger numbers of AuNPs on the tubular origami than on the rectangular origami. The AuNPs show higher addressability on the tubular origami, likely because the large curvature of the tubular origami decreases the steric hindrance between the AuNPs and hence allows more AuNPs to localize on the origami.

The assembly yield and spatial control of the AuNPs on the origami could be further improved by using smaller AuNPs (6–8 nm), which would decrease the steric hindrance and charge repulsion, or by enlarging the separation between binding sites in the design. The conformation of our 3D AuNP helices bears a strong resemblance to well-known chiral molecules such as DNA or proteins, leading to plasmonic analogues of chiral materials. To characterize the optical response of the AuNP helices, CD measurements were carried out in a 1× TAE/Mg^{2+} buffer with a quartz cuvette (0.2 cm path length) using a J-810 CD spectrometer. The wavelength range was 400–750 nm, and the scan rate was 50 nm/min. As shown by the red curve in Figure 4, the CD spectrum of the 10 nm AuNP helices exhibits

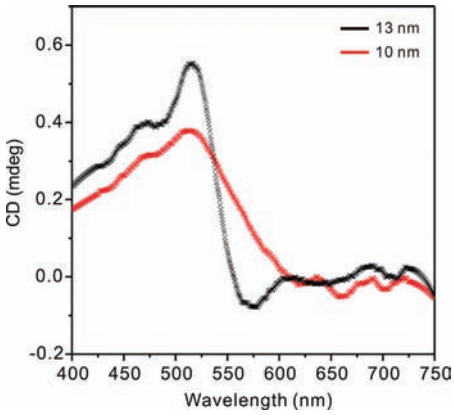

Figure 4. Measured CD spectra of helices assembled using 10 nm (red) and 13 nm (black) AuNPs.

the characteristic peak-dip CD line shape in the vicinity of the plasmonic resonance of the AuNPs (~525 nm), demonstrating the plasmonic chiral response of our structure. In addition, we fabricated left-handed 13 nm AuNP helices (see the Supporting Information), which gave rise to much stronger CD signals as a result of the greater oscillator strength of the larger AuNPs (black curve).

In conclusion, we have introduced a unique and simple way to construct 3D AuNP helices using DNA origami. 2D rectangular DNA origami was utilized to organize AuNPs precisely at well-defined binding sites along two linear chains. 3D AuNP helices were obtained by rationally rolling and stapling the 2D rectangular origami sheets. The structural parameters of the 3D AuNP helices, such as the diameter and axial length, could be tuned by modifying the width, length, and stapling position of the rectangular DNA origami template. The pitch of the 3D AuNP helices could be adjusted by varying the AuNP chain number on the origami. Furthermore, the coupling strength between the AuNPs could be increased through Au or Ag electroless deposition in that it can enlarge the size of the AuNPs and simultaneously can reduce the AuNP spacing on the DNA origami. This would lead to fully engineerable plasmonic chiral nanomaterials. Enlargement of AuNPs through electroless deposition to control the plasmonic chiral response has recently been demonstrated by Kuzyk et al.[32]

Our strategy opens up a number of possibilities for the realization of programmable 3D plasmonic structures with

dx.doi.org/10.1021/ja209861x | J. Am. Chem.Soc. 2012, 134, 146–149

desired optical properties. These 3D chiral nanomaterials might enable a new generation of 3D plasmon rulers in that CD spectra are notably sensitive to 3D conformational changes.[33] For example, subtle spatial changes could be reported in real time by monitoring changes in the CD spectrum resulting from the binding or cleavage of a specific staple strand on the origami by enzymes or proteins.[34] Also, rationally designed DNA origami templates could be further modified to accomplish precise 3D organization of multiple components (e.g., different metallic NPs, magnetic NPs, quantum dots, and proteins) for various functionalities and applications.[35]

■ ASSOCIATED CONTENT

Supporting Information

Experimental section, designs and sequences, and additional TEM images. This material is available free of charge via the Internet at http://pubs.acs.org.

■ AUTHOR INFORMATION

Corresponding Author

nl7@rice.edu; dingbq@nanoctr.cn

■ ACKNOWLEDGMENTS

The authors are grateful for financial support from the National Basic Research Program of China (973 Program, 2012CB934000), the National Natural Science Foundation of China (21173059, 91127021), and the 100-Talent Program of the Chinese Academy of Sciences (B.D.). N.L. was financially supported by a K. Bala Texas Instruments Visiting Professorship in Electrical and Computer Engineering at Rice University.

■ REFERENCES

(1) Seeman, N. C. *Nature* **2003**, *421*, 427.
(2) Seeman, N. C. *Annu. Rev. Biochem.* **2010**, *79*, 65.
(3) Lin, C.; Liu, Y.; Yan, H. *Biochemistry* **2009**, *48*, 1663.
(4) Torring, T.; Voigt, N. V.; Nangreave, J.; Yan, H.; Gothelf, K. *Chem. Soc. Rev* **2011**, *40*, 5636.
(5) Rothemund, P. W. K. *Nature* **2006**, *440*, 297.
(6) Andersen, E. S.; Dong, M.; Nielsen, M. M.; Jahn, K.; Subramani, R.; Mamdouh, W.; Golas, M. M.; Sander, B.; Stark, H.; Oliveira, C. L.; Pedersen, J. S.; Birkedal, V.; Besenbacher, F.; Gothelf, K. V.; Kjems, J. *Nature* **2009**, *459*, 73.
(7) Ke, Y.; Sharma, J.; Liu, M.; Jahn, K.; Liu, Y.; Yan, H. *Nano Lett.* **2009**, *9*, 2445.
(8) Douglas, S.; Dietz, H.; Liedl, T.; Högberg, B.; Graf, F.; Shih, W. *Nature* **2009**, *459*, 414.
(9) Dietz, H.; Douglas, S. M.; Shih, W. M. *Science* **2009**, *325*, 725.
(10) Ke, Y.; Douglas, S. M.; Liu, M.; Sharma, J.; Cheng, A.; Leung, A.; Liu, Y.; Shih, W. M.; Yan, H. *J. Am. Chem. Soc.* **2009**, *131*, 15903.
(11) Liedl, T.; Högberg, B.; Tytell, J.; Ingber, D. E.; Shih, W. M. *Nat. Nanotechnol.* **2010**, *5*, 520.
(12) Han, D.; Pal, S.; Nangreave, J.; Deng, Z.; Liu, Y.; Yan, H. *Science* **2011**, *332*, 342.
(13) Ke, Y.; Lindsay, S.; Chang, Y.; Liu, Y.; Yan, H. *Science* **2008**, *319*, 180.
(14) Maune, H. T.; Han, S.-p.; Barish, R. D.; Bockrath, M.; Goddard, W. A. III; Rothemund, P. W. K.; Winfree, E. *Nat. Nanotechnol.* **2010**, *5*, 61.
(15) Ding, B. Q.; Deng, Z. T.; Yan, H.; Cabrini, S.; Zuckermann, R. N.; Bokor, J. *J. Am. Chem. Soc.* **2010**, *132*, 3248.
(16) Stephanopoulos, N.; Liu, M.; Tong, G. J.; Li, Z.; Liu, Y.; Yan, H.; Francis, M. B. *Nano Lett.* **2010**, *10*, 2714.
(17) Pal, S.; Deng, Z.; Ding, B.; Yan, H.; Liu, Y. *Angew. Chem., Int. Ed.* **2010**, *49*, 2700.
(18) Gu, H.; Chao, J.; Xiao, S. J.; Seeman, N. C. *Nature* **2010**, *465*, 202.
(19) Lund, K.; Manzo, A. J.; Dabby, N.; Michelotti, N.; Johnson-Buck, A.; Nangreave, J.; Taylor, S.; Pei, R.; Stojanovic, M. N.; Walter, N. G.; Winfree, E.; Yan, H. *Nature* **2010**, *465*, 206.
(20) Voigt, N. V.; Tørring, T.; Rotaru, A.; Jacobsen, M. F.; Ravnsbæk, J. B.; Subramani, R.; Mamdouh, W.; Kjems, J.; Mokhir, A.; Besenbacher, F.; Gothelf, K. V. *Nat. Nanotechnol.* **2010**, *5*, 200.
(21) Bui, H.; Onodera, C.; Kidwell, C.; Tan, Y.; Graugnard, E.; Kuang, W.; Lee, J.; Knowlton, W. B.; Yurke, B.; Hughes, W. L. *Nano Lett.* **2010**, *10*, 3367.
(22) Liu, N.; Guo, H.; Fu, L.; Kaiser, S.; Schweizer, H.; Giessen, H. *Nat. Mater.* **2008**, *7*, 31.
(23) Liu, N.; Liu, H.; Zhu, S.; Giessen, H. *Nat. Photonics* **2009**, *3*, 157.
(24) Sharma, J.; Chhabra, R.; Anderson, C. S.; Gothelf, K. V.; Yan, H.; Liu, Y. *J. Am. Chem. Soc.* **2008**, *130*, 7820.
(25) Zhao, Z.; Liu, Y.; Yan, H. *Angew. Chem., Int. Ed* **2011**, *50*, 2041.
(26) Pilo-Pais, M.; Goldberg, S.; Samano, E.; Labean, T. H.; Finkelstein, G. *Nano Lett.* **2011**, *11*, 3489.
(27) Gansel, J. K.; Thiel, M.; Rill, M. S.; Decker, M.; Bade, K.; Saile, V.; von Freymann, G.; Linden, S.; Wegener, M. *Science* **2009**, *325*, 1513. Radke, A.; Gissibl, T.; Klotzbuecher, T.; Braun, P. V.; Giessen, H. *Adv. Mater.* **2011**, *23*, 3018.
(28) Fan, Z.; Govorov, A. O. *Nano Lett.* **2010**, *10*, 2580. Fan, Z.; Govorov, A. O. *J. Phys. Chem. C* **2011**, *115*, 13254.
(29) Chen, C.; Zhang, P.; Rosi, N. L. *J. Am. Chem. Soc.* **2008**, *130*, 13333.
(30) Sharma, J.; Chhabra, R.; Cheng, A.; Brownell, J.; Liu, Y.; Yan, H. *Science* **2009**, *323*, 112.
(31) Mastroianni, A. J.; Claridge, S. A.; Alivisatos, A. P. *J. Am. Chem. Soc.* **2009**, *131*, 8455.
(32) Kuzyk, A.; Schreiber, R.; Fan, Z.; Pardatscher, G.; Roller, E. M.; Högele, A.; Simmel, F. C.; Govorov, A. O.; Liedl, T. 2011, arXiv:1108.3752v1. arXiv.org e-Print archive. http://arxiv.org/abs/1108.3752v1 (accessed Oct 20, 2011).
(33) Liu, N.; Hentschel, M.; Weiss, T.; Alivisatos, A. P.; Giessen, H. *Science* **2011**, *332*, 1407.
(34) Reinhard, B. M.; Sheikoleslami, S.; Mastorianni, A.; Alvisatos, A. P.; Liphardt, J. *Proc. Natl. Acad. Sci. U.S.A.* **2007**, *104*, 2667.
(35) Tan, S. J.; Campolongo, M. J.; Luo, D.; Cheng, W. *Nat. Nanotechnol.* **2011**, *6*, 268.